Nucleus-nucleus cold fusion reactions analyzed with the *l*-dependent "fusion by diffusion" model

T. Cap and K. Siwek-Wilczyńska
Institute of Experimental Physics, Faculty of Physics, University of Warsaw, Hoża 69, PL-00-681 Warsaw, Poland

J. Wilczyński
Andrzej Sołtan Institute for Nuclear Studies, PL-05-400 Otwock-Świerk, Poland

(Received 7 February 2011; published 6 May 2011)

We present a modified version of the Fusion by Diffusion (FBD) model aimed at describing the synthesis of superheavy nuclei in cold fusion reactions, in which a low excited compound nucleus emits only one neutron. The modified FBD model accounts for the angular momentum dependence of three basic factors determining the evaporation residue cross section: the capture cross section $\sigma_{\rm cap}(l)$, the fusion probability $P_{\rm fus}(l)$, and the survival probability $P_{\rm surv}(l)$. The fusion hindrance factor, the inverse of $P_{\rm fus}(l)$, is treated in terms of thermal fluctuations in the shape degrees of freedom and is expressed as a solution of the Smoluchowski diffusion equation. The l dependence of $P_{\rm fus}(l)$ results from the l-dependent potential energy surface of the colliding system. A new parametrization of the distance of starting point of the diffusion process is introduced. An analysis of a complete set of 27 excitation functions for production of superheavy nuclei in cold fusion reactions, studied in experiments at GSI Darmstadt, RIKEN Tokyo, and LBNL Berkeley, is presented. The FBD model satisfactorily reproduces shapes and absolute cross sections of all the cold fusion excitation functions. It is shown that the peak position of the excitation function for a given $1n$ reaction is determined by the Q value of the reaction and the height of the fission barrier of the final nucleus. This fact could possibly be used in future experiments (with well-defined beam energy) for experimental determination of the fission barrier heights.

DOI: 10.1103/PhysRevC.83.054602 PACS number(s): 25.70.Jj, 25.70.Gh

I. INTRODUCTION

This article presents a new theoretical analysis of the complete set of experimental data on synthesis of superheavy nuclei in *cold* fusion reactions, including measurements for 27 reactions carried out at GSI Darmstadt, RIKEN Tokyo, and LBNL Berkeley. Very heavy nuclei in the range of atomic numbers $Z = 104$–113 were produced in these experiments by bombarding strongly bound target nuclei, ^{208}Pb and ^{209}Bi, with the variety of projectiles ranging from ^{48,50}Ti to ^{70}Zn. In all these reactions only one neutron is evaporated from the compound nucleus to cool it down to its ground state. This makes it considerably easier to calculate the probability of the statistical deexcitation of the compound nucleus and thus focus on disentangling the physics of amalgamation of very heavy nuclear systems.

For the analysis we used the Fusion by Diffusion (FBD) model developed by Świątecki *et al.* [1,2]. A smaller set of cold fusion reactions had already been analyzed with the original version of the FBD model [2]. In this article an up-to-date set of $1n$ evaporation-residue excitation functions, including new LBNL and RIKEN data, is reanalyzed by using a modified version of the FBD model. The most important modifications consist in the inclusion of the angular momentum in the description of the potential energy surface of the interacting nucleus-nucleus system on its way to overcome the fusion barrier as well as in the description of the deexcitation of the compound nucleus. Moreover, an individual treatment of the geometry of the rapid growth of the neck between the target and projectile is proposed for each individual reaction. This enables one to establish a phenomenological parametrization of this very critical constituent of fusion of very heavy systems, decisively influencing the cross sections.

In the following we give an overview of the FBD model together with the information on all the modifications implemented to the model described in Ref. [2].

II. BASIC SCHEME AND MODIFICATIONS OF THE FUSION BY DIFFUSION MODEL

For each value of the entrance-channel angular momentum, the partial evaporation-residue cross section $\sigma_{\rm ER}(l)$ for production of a given final nucleus in its ground state is factorized in the FBD model as the product of the partial capture cross section $\sigma_{\rm cap}(l) = \pi\lambda\!\!\!^{-2}(2l+1)T(l)$, the fusion probability $P_{\rm fus}(l)$, and the survival probability $P_{\rm surv}(l)$:

$$\sigma_{\rm ER} = \pi\lambda\!\!\!^{-2}\sum_{l=0}^{\infty}(2l+1)T(l)P_{\rm fus}(l)P_{\rm surv}(l). \qquad (1)$$

The capture transmission coefficients $T(l)$ are calculated in a simple sharp cutoff approximation: $T(l) = 1$ for $l \leqslant l_{\rm max}$, and $T(l) = 0$ for $l > l_{\rm max}$, where $l_{\rm max}$ is determined by the capture cross section $\sigma_{\rm cap}$, i.e., the cross section of overcoming the interaction barrier at a given bombarding energy $E_{\rm c.m.}$,

$$\sigma_{\rm cap} = \pi\lambda\!\!\!^{-2}\sum_{l=0}^{l_{\rm max}}(2l+1) = \frac{\pi\hbar^2}{2\mu E_{\rm c.m.}}(l_{\rm max}+1)^2, \qquad (2)$$

where $\lambda\!\!\!^{-}$ is the wavelength, $\lambda\!\!\!^{-2} = \hbar^2/2\mu E_{\rm c.m.}$, and μ is the reduced mass of the colliding system. For determination of $\sigma_{\rm cap}$, see the next subsection.

Two other factors in Eq. (1) are defined as follows: $P_{\rm fus}(l)$ is the probability that the colliding system, after reaching the capture configuration, will eventually overcome the fission barrier and fuse, thus avoiding reseparation, and $P_{\rm surv}(l)$ is

the probability for the compound nucleus to decay to the ground state of the final residual nucleus via evaporation of light particles and γ rays, thus surviving fission.

A. The capture cross section

The capture cross section $\sigma_{\rm cap}$ is the cross section for *overcoming* the entrance channel Coulomb barrier and is given by the "diffused barrier formula" [2,3] based on the assumption of a Gaussian distribution of barriers around a mean B_0:

$$\sigma_{\rm cap} = \pi \tilde{R}^2 \frac{w}{E_{\rm c.m.}\sqrt{2\pi}}[X\sqrt{\pi}(1+{\rm erf}X)+\exp(-X^2)], \quad (3)$$

where

$$X = \frac{E_{\rm c.m.} - B_0}{w\sqrt{2}}, \quad (4)$$

and erf$X$ is the Gaussian error integral of the argument X. Here the parameter B_0 denotes the mean value of the barrier distribution and w its width. Both these parameters, as well as the cross section normalization parameter $\tilde{R}$, had been determined from analysis of fusion excitation functions for about 50 nuclear systems [3]. The resulting mean barrier parameter B_0 was parameterized by a cubic polynomial:

$$B_0 = 0.853315z + 0.0011695z^2 - 0.000001544z^3 \ {\rm MeV}, \quad (5)$$

where $z = Z_1Z_2/(A_1^{1/3} + A_2^{1/3})$. The normalization $\tilde{R}$ parameter was taken as $\tilde{R} = 1.16(A_1^{1/3} + A_2^{1/3})$ fm [3], and the width w was calculated as described in Ref. [2], but with some minor modifications:

$$\omega = C B_0\sqrt{\omega_1^2 + \omega_2^2 + \omega_0^2}, \quad (6)$$

where $\omega_i = R_i^2\beta_{2i}^2/4\pi$, with the radii R_1 and R_2 defined as $R_i = 1.15A_i^{1/3}$ and their quadrupole deformation parameters β_2 taken from Ref. [4]. In this notation the parameters C and ω_0 were found to be $C = 0.0421$ fm^{-1} and $\omega_0 = 0.531$ fm.

B. The fusion hindrance factor

Contrary to lighter systems, in collisions of heavy nuclear systems the fusion probability $P_{\rm fus}$ is not equal to unity. For the heaviest systems $P_{\rm fus}$ is reduced by several orders of magnitude due to the fact that the fusing system must find its way from the configuration of two touching nuclei at the Coulomb barrier to the saddle point of the compound nucleus, which is located well inside the Coulomb barrier configuration. It is assumed in the model that after the contact at the Coulomb barrier configuration, the neck connecting the two nuclei grows rapidly at an approximately fixed mass asymmetry and constant length of the system. This "neck zip" is much faster than the characteristic speeds of other collective degrees of freedom due to a large savings in surface energy during the filling in of the crevice between the surfaces of the touching nuclei. The neck zip is expected to carry the system toward the bottom of the asymmetric fission valley corresponding to the initial projectile-target mass asymmetry. This is the "injection point," from where the system starts its climb uphill over the saddle in the process of thermal fluctuations in the shape degrees of freedom. Obviously, it is a simplification to assume that there is no contribution to the probability of overcoming the saddle point directly from the fast neck-zip stage. Also, it is largely idealized to assume that the point at which the diffusion effectively begins is just at one location of the asymmetric fission valley, but the crudeness of this assumption is contained in treating the location of the injection point as an *adjustable* parameter. By idealizing the process of thermal fluctuations as a one-dimensional diffusion over a parabolic barrier, one finds [1,2,5] the probability that the system injected on the outside the saddle point at an energy H below the top will achieve fusion is

$$P_{\rm fus} = \tfrac{1}{2}(1 - {\rm erf}\sqrt{H/T}), \quad (7)$$

where T is the temperature of the fusing system, which decreases during the uphill diffusion from an initial temperature at the injection point $T_{\rm inj}$ to a lower temperature at the top of the saddle point $T_{\rm saddle}$. It is reasonable to use in Eq. (7) the geometrical mean between these two values. The energy threshold H opposing fusion in the diffusion process is calculated using simple algebraical expressions that approximate the potential energy surface (see Sec. II C). The corresponding values of the rotational energy at the injection point and at the symmetric saddle point are calculated assuming moments of inertia as specified in Sec. II D. The fact that H depends on the angular momentum causes that for higher partial waves, fusion is strongly reduced in comparison with central collisions (the rotational energy of the saddle point rises faster with l than the rotational energy at the injection point). The effective energy thresholds that oppose fusion, $H(l)$, are typically of several MeV, ranging in cold fusion reactions (see Sec. IV) from about 2 to 7 MeV, thus resulting in a considerable hindrance of the fusion probability $P_{\rm fus}$, by two to six orders of magnitude, respectively, especially for the heaviest fusing systems.

C. The deformation energy along the asymmetric fission valley

The macroscopic (liquid drop) part of the potential energy for the colliding projectile-plus-target system and for the fissioning compound nucleus was tabulated in Ref. [6] as functions of three degrees of freedom: elongation, asymmetry, and neck size. Based on this approach, an algebraic expression for the macroscopic deformation energy along the asymmetric fission valley was obtained in Ref. [2]. This algebraic approximation was later improved. Therefore in the following we give the complete set of the modified equations.

We calculate the deformation energy of the drop $E_{\rm def}$, originally spherical with the radius R, parameterized by two spheres with radii R_1 and R_2 connected smoothly by a portion of a spheroid, cone, or hyperboloid [6], expressed in units of the surface energy $E_{\rm surf}$ of the spherical shape [2,7],

$$\xi = E_{\rm def}/E_{\rm surf}. \quad (8)$$

Let L stand for the total length of the dinuclear shape, and s for the surface separation between the two spheres, $s = L - 2(R_1 + R_2)$. The following quadratic approximation to the deformation energy ξ along the asymmetric fission valley,

in dependence on the variable $S = s/R$, was found for the range of *outer* configurations $L > 2(R_1 + R_2)$:

$$\xi_> = a + bS + cS^2. \tag{9}$$

The parameters a, b, and c are expressed as follows:

$$a = \alpha_1 + \alpha_2 t + \alpha_3 t^2, \tag{10}$$
$$b = \beta_1 + \beta_2 t + \beta_3 t^2, \tag{11}$$
$$c = \gamma_1 + \gamma_2 t + \gamma_3 t^2, \tag{12}$$

where

$$\alpha_1 = -0.00564 - 0.01936\exp(-D/0.02240), \tag{13}$$
$$\alpha_2 = 0.05122 + 0.11931\exp(-D/0.03800), \tag{14}$$
$$\alpha_3 = -0.07424 + 0.95959D, \tag{15}$$
$$\beta_1 = -0.06080 + 1.37825D - 10.7077D^2, \tag{16}$$
$$\beta_2 = 0.27691 - 2.93119D + 12.60944D^2, \tag{17}$$
$$\beta_3 = -0.02398 - 1.14854D, \tag{18}$$
$$\gamma_1 = -0.02722 + 0.2231D, \tag{19}$$
$$\gamma_2 = 0.02050 + 0.32122D, \tag{20}$$
$$\gamma_3 = 0.03843 + 1.03731D. \tag{21}$$

The following notation is used in the above formulas: $t = 1 - x$, where x is the fissility parameter as defined in Ref. [7], and $D = \Delta^2$, where $\Delta = (R_1 - R_2)/(R_1 + R_2)$ is the asymmetry parameter used in Ref. [6].

In the interval of lengths between contact, $L = 2(R_1 + R_2)$, and the spherical shape at $L = 2R$ (i.e., for negative values of s) we shall use instead of Eq. (9) the cubic

$$\xi_< = p(S - S_0)^2 - q(S - S_0)^3, \tag{22}$$

where S_0 corresponds to a value of S for the spherical compound nucleus

$$S_0 = \frac{2R - 2(R_1 + R_2)}{R} = 2 - \frac{4}{(2 + 6D)^{1/3}}. \tag{23}$$

From a smooth junction of Eqs. (9) and (22) for $S = 0$ we find

$$p = \frac{b}{S_0} + \frac{3a}{S_0^2}, \tag{24}$$
$$q = -\frac{b}{S_0^2} - \frac{2a}{S_0^3}. \tag{25}$$

The above formulas of the algebraic approximation to the macroscopic deformation energy have been tested for adequate accuracy in the range $0.85 < x < 1.05$ and $-0.25 < \Delta < 0.25$.

D. Macroscopic saddle and rotational energy

Equations (9) and (22) were used to calculate the deformation energy of the system at the injection point in the *asymmetric* fission valley (corresponding to the initial projectile-target mass asymmetry) and also the deformation energy of the saddle point that separates the equilibrium hollow of the compound nucleus and the *symmetric* fission valley, $\Delta = 0$. The deformation energy (zero for the spherical shape) was added to the macroscopic energy of a spherical nucleus (calculated with the Thomas-Fermi model [8]) to obtain the *macroscopic* energy of the system for a given shape. The ground-state energies of the compound nucleus (accounting for the ground-state shell effect [4]) were taken from Ref. [8].

In the present (modified) version of the FBD model the rotational energy at both the injection point and the saddle point was calculated by assuming the rigid-body moments of inertia for the respective shapes. For the injection point

$$\mathcal{I}_{\rm inj} = \mu r^2 + 2/5 M_P R_P^2 + 2/5 M_T R_T^2, \tag{26}$$

where M_P and M_T and R_P and R_T are masses and radii of the projectile and target, respectively, μ is the reduced mass of the projectile and target system, and r is the distance between the projectile and target at the injection point. For the saddle configuration the moment of inertia is calculated for ellipsoidal shape

$$\mathcal{I}_{sd} \approx \tfrac{1}{5} M R^2[(1+\alpha)^2 + (1+\alpha)^{-1}] + 2Mb_f^2, \tag{27}$$

where $\alpha = (R_{\rm max} - R)/R$ is the deformation of the (axially symmetric) ellipsoid defined by its semimajor axis $R_{\rm max}$ and the radius R of a sphere of the same volume. The last term in Eq. (27) accounts [9] for the diffuseness $b_f \approx 1$ fm of the mass distribution of the fissioning nucleus of mass M.

The difference of the potential energy between the saddle point and the injection point, corrected for the respective rotational energies, determine the barrier height H opposing fusion; see Eq. (7).

A comment is necessary on how the energy of the saddle point can be estimated in case of superheavy compound systems with fissility approaching the limit $x = 1$, for which the macroscopic saddle tends to have nearly spherical configuration with the disappearing macroscopic fission barrier. As these heavy nuclei are entirely stabilized by the shell effect, their saddle-point deformation is not determined by their macroscopic properties. Macroscopic-microscopic calculations [10] show that this deformation may be quite large, especially if the ground state is deformed. In the present study, the energy of the saddle point was calculated as the *macroscopic* energy of the deformed nucleus along the symmetric ($\Delta = 0$) fission valley assuming the saddle-point deformation following from a systematics of macroscopic-microscopic calculations of Muntian *et al.* [10]. An approximate rule resulting from these calculations for superheavy nuclei of $Z = 106$–120 is that for superheavy nuclei that are deformed in their ground state the saddle-point deformation is equal to $\alpha_{\rm sd} \approx 0.35$, while for nuclei that are spherical in the ground state $\alpha_{\rm sd} \approx 0.18$. A given nucleus is assigned to be deformed when the theoretical [4] rms deformation parameter of its ground state $\beta_{\rm rms} = \sqrt{\beta_2^2 + \beta_4^2 + \beta_6^2}$ is larger than 0.15, otherwise the nucleus is assumed to be spherical. The deformation parameter $\alpha_{\rm sd}$ (at the saddle) converts into the separation parameter $S_{\rm sd}$ (also at the saddle) via the relation $\alpha_{\rm sd} = (S_{\rm sd} - S_0)/2$.

For completeness, it should be noted that the moment of inertia of the compound nucleus in its ground state (used to calculate the rotational energy of the decaying compound nucleus; see next section) is also calculated as for the ellipsoidal shape with Eq. (27). The effective deformation parameter $\alpha_{\rm gs}$ is then defined [9] by theoretical ground-state

deformations β_2, β_4, and β_6 taken from Möller *et al.* [4]:

$$\alpha_{gs} = \sqrt{\frac{5}{4\pi}}\beta_2 + \sqrt{\frac{9}{4\pi}}\beta_4 + \sqrt{\frac{13}{4\pi}}\beta_6. \quad (28)$$

III. SURVIVAL PROBABILITY

The competition between deexcitation of the compound nucleus by neutron emission and fission is treated by standard methods. In cold fusion reactions, when only one neutron is emitted from the compound nucleus, the survival probability $P_{\rm surv}$ in Eq. (1) is given by the ratio of the neutron decay width Γ_n and the total neutron plus fission width, $\Gamma_{\rm tot} \approx \Gamma_n + \Gamma_f$, multiplied by the probability $P_<$ that the excitation energy (after the emission of the neutron) is less than the threshold for second chance fission or second neutron emission:

$$P_{\rm surv} = \frac{\Gamma_n}{\Gamma_n + \Gamma_f} P_<. \quad (29)$$

Traditionally, the neutron width is calculated by using the Weisskopf formula,

$$\Gamma_n = \frac{g_n m_n \sigma_n}{\pi^2 \hbar^2 \rho_A(E_A^*)} \int_0^{E_{A-1}^{*\rm max}} \rho_{A-1}\left(E_{A-1}^{*\rm max} - \epsilon_n\right)\epsilon_n \, d\epsilon_n, \quad (30)$$

where the product of the kinetic energy of the emitted neutron ϵ_n and the level density of the daughter nucleus of mass number $(A-1)$ is integrated over ϵ_n in the range from 0 to a maximum possible energy $E_{A-1}^{*\rm max} = E_A^* - B_n^A - E_{A-1}^{\rm rot} - E_{A-1}^{\rm pair}$, where E_A^* is the excitation energy of the parent nucleus, B_n^A is the neutron binding energy in the parent nucleus, and $E_{A-1}^{\rm rot}$ and $E_{A-1}^{\rm pair}$ are the rotational and pairing energies in the daughter nucleus, respectively. In the preintegral factor of Eq. (30), $g_n = 2$ is the neutron spin degeneracy, m_n is the neutron mass, $\sigma_n \approx \pi r_0^2 A^{2/3}$ with $r_0 \approx 1.45$ fm [11] stands for the cross section for neutron capture, the inverse of neutron evaporation, and $\rho_A(E_A^*)$ is the level density of the parent nucleus at the initial excitation energy E_A^*.

The fission width is given by the transition state theory,

$$\Gamma_f = \frac{1}{2\pi\rho_A(E_A^*)} \int_0^{E_{A,\rm sd}^{*\rm max}} \rho_{A,\rm sd}\left(E_{A,\rm sd}^{*\rm max} - K\right) dK, \quad (31)$$

where the level density $\rho_{A,\rm sd}$ of the fissioning nucleus of mass A and excitation energy at the saddle point, $E_{A,\rm sd}^* = E_{A,\rm sd}^{*\rm max} - K$, is integrated over the kinetic energy K in the fission degree of freedom in the range of the excitation energy at the saddle configuration from 0 to a maximum possible thermal excitation energy $E_{A,\rm sd}^{*\rm max} = E_A^* - B_f^A - E_{A,\rm sd}^{\rm rot} - E_A^{\rm pair}$, where $E_{A,\rm sd}^{\rm rot}$ and $E_A^{\rm pair}$ are the rotational and pairing energies of the fissioning nucleus, respectively, and B_f^A is the fission barrier given by the difference of the potential energy at the saddle point of the fissioning nucleus of mass number A and the energy of that nucleus in its ground state, $B_f^A = E_{A,\rm sd} - E_{A,\rm gs}$.

The factor $P_<$ in Eq. (29) represents the probability that evaporation of a neutron will bring the final nucleus $(A-1)$ below its threshold for the second chance fission, $E_{A-1}^{*\rm thr}(f) = B_f^{A-1} + E_{(A-1)\rm sd}^{\rm rot} - E_{A,\rm sd}^{\rm rot}$, or the threshold for emission of a second neutron, $E_{A-1}^{*\rm thr}(n) = B_n^{A-1} + E_{(A-2)\rm gs}^{\rm rot} - E_{(A-1)\rm gs}^{\rm rot}$, whatever is lower. Therefore

$$P_< = \frac{\int_{\epsilon_{\rm thr}}^{E_{A-1}^{*\rm max}} \rho_{A-1}\left(E_{A-1}^{*\rm max} - \epsilon_n\right)\epsilon_n \, d\epsilon_n}{\int_0^{E_{A-1}^{*\rm max}} \rho_{A-1}\left(E_{A-1}^{*\rm max} - \epsilon_n\right)\epsilon_n \, d\epsilon_n}, \quad (32)$$

where the threshold value of the variable ϵ_n equals $\epsilon_{\rm thr} = E_{A-1}^{*\rm max} - E_{A-1}^{*\rm thr}$ or $\epsilon_{\rm thr} = 0$ if $E_{A-1}^{*\rm max} - E_{A-1}^{*\rm thr} \leqslant 0$. Here $E_{A-1}^{*\rm thr} = \min[E_{A-1}^{*\rm thr}(f), E_{A-1}^{*\rm thr}(n)]$.

In Ref. [2] a close form expression for $P_<$ based on the integration of the Maxwellian shape of the integrand in Eq. (32) was used. In the present work we used exact integrals in Eq. (32). This resulted in a more accurate description of the high-energy part of energy distributions of the fusion cross section.

It should be noted that in all calculations of the survival probability $P_{\rm surv}$, the excitation energy of a given nucleus was evaluated with respect to its ground state energy which, if unknown experimentally, was taken from the Thomas-Fermi-model mass tables of Myers and Swiatecki [8]. For example, the excitation energy of the compound nucleus, $E_A^* = E_{\rm c.m.} - Q_{\rm fusion} = E_{\rm c.m.} - (M_P + M_T - M_A)c^2$, was calculated assuming experimental masses of the projectile and target, M_P and M_T, and the theoretical [8] mass of the compound nucleus M_A.

A. Level densities and shell effects

To calculate the survival probability $P_{\rm surv}$ discussed in this section, we used the Fermi-gas-model level densities

$$\rho = \text{const.} \times \exp 2\sqrt{aU}, \quad (33)$$

where U is the excitation energy E^* of a nucleus of a given shape corrected for its rotational energy $E^{\rm rot}$ and pairing energy $E^{\rm pair}$, $U = E^* - E^{\rm rot} - E^{\rm pair}$, where $E^{\rm pair} = 21/\sqrt{A}$ MeV, $10.5/\sqrt{A}$ MeV and 0 for even-even, odd, and odd-odd nuclei, respectively [12]. Well-tested and realistic values of a smooth, shape-dependent level density parameter $\tilde{a}$ proposed by Reisdorf [12] was used:

$$\tilde{a} = a_v A + a_s A^{2/3} B_S + a_c A^{1/3} B_K, \quad (34)$$

where $a_v = 0.0696$ MeV^{-1}, $a_s = 0.1801$ MeV^{-1}, and $a_c = 0.1644$ MeV^{-1}, and B_S and B_K are the surface and curvature functions [9] that approximately determine the shape dependence of the level density on the deformation variable α used in the calculations of the macroscopic energy and moments of inertia (see Sec.II.D):

$$B_S = 1 + (0.6416\alpha - 0.1421\alpha^2)^2, \quad (35)$$

$$B_K = 1 + (0.6542\alpha - 0.0483\alpha^2)^2. \quad (36)$$

As demonstrated by Ignatyuk *et al.* [13], the level densities determined experimentally can be well reproduced assuming that the smooth value of the level density parameter $\tilde{a}$ is modified due to shell effects according to the formula

$$a = \tilde{a}\left\{1 + \frac{E_{\rm shell}}{U}[1 - \exp(-U/E_D)]\right\}, \quad (37)$$

where $E_{\rm shell}$ is the shell correction energy, and E_D is a parameter determining the damping of shell effects with the increasing effective excitation energy U. According to the

TABLE I. List of cold fusion reactions studied in experiments at GSI Darmstadt, RIKEN Tokyo, and LBNL Berkeley. The reactions are arranged according to Z of the compound nucleus and the Coulomb parameter $z = Z_1Z_2/(A_1^{1/3} + A_2^{1/3})$. The table contains respective values of the ground-state Q value, calculated for the Thomas-Fermi mass tables of Myers and Swiatecki [8]. Target thicknesses quoted in original papers and used to average the theoretical excitation functions (see text) are also listed.

Reaction	Ref.	Coulomb parameter z	Q value (MeV)	Target thickness (μg/cm^2)
$Z = 104$				
^{208}Pb(^{50}Ti, n)^{257}Rf	[15,16]	187.74	−177.74	400
^{208}Pb(^{50}Ti, n)^{257}Rf	[17]	187.74	−177.74	104
^{208}Pb(^{48}Ti, n)^{255}Rf	[17]	188.72	−173.03	470
$Z = 105$				
^{209}Bi(^{50}Ti, n)^{258}Db	[16,18]	189.84	−180.02	450
^{209}Bi(^{50}Ti, n)^{258}Db	[19]	189.84	−180.02	441
^{208}Pb(^{51}V, n)^{258}Db	[19]	195.78	−184.28	470
$Z = 106$				
^{208}Pb(^{54}Cr, n)^{261}Sg	[15,16]	202.79	−195.48	450
^{208}Pb(^{52}Cr, n)^{259}Sg	[20]	203.78	−192.34	470
$Z = 107$				
^{209}Bi(^{54}Cr, n)^{262}Bh	[21]	205.06	−198.18	441
^{209}Bi(^{54}Cr, n)^{262}Bh	[22]	205.06	−198.18	390–660
^{209}Bi(^{52}Cr, n)^{260}Bh	[23]	206.06	−195.59	441
^{208}Pb(^{55}Mn, n)^{262}Bh	[21,24]	210.73	−202.45	470
$Z = 108$				
^{208}Pb(^{58}Fe, n)^{265}Hs	[15,16]	217.64	−213.48	450
^{208}Pb(^{56}Fe, n)^{263}Hs	[25]	218.65	−210.86	250
$Z = 109$				
^{209}Bi(^{58}Fe, n)^{266}Mt	[16,26]	220.08	−216.80	450
^{208}Pb(^{59}Co, n)^{266}Mt	[27]	225.50	−220.36	460
$Z = 110$				
^{208}Pb(^{64}Ni, n)^{271}Ds	[15,16]	231.34	−232.39	450
^{208}Pb(^{64}Ni, n)^{271}Ds	[28,29]	231.34	−232.39	500
^{208}Pb(^{64}Ni, n)^{271}Ds	[30,31]	231.34	−232.39	190–270
^{207}Pb(^{64}Ni, n)^{270}Ds	[32]	231.56	−231.92	435
^{208}Pb(^{62}Ni, n)^{269}Ds	[16]	232.32	−231.33	450
$Z = 111$				
^{209}Bi(^{64}Ni, n)^{272}Rg	[16]	233.93	−236.07	450
^{209}Bi(^{64}Ni, n)^{272}Rg	[31,33]	233.93	−236.07	280
^{208}Pb(^{65}Cu, n)^{272}Rg	[29]	239.10	−239.72	470
$Z = 112$				
^{208}Pb(^{70}Zn, n)^{277}Cn	[15,16]	244.87	−251.03	450
^{208}Pb(^{70}Zn, n)^{277}Cn	[34]	244.87	−251.03	450
$Z = 113$				
^{209}Bi(^{70}Zn, n)^{278}113	[35,36]	247.62	−254.77	450

parametrization tested by Reisdorf [12], $E_D = 18.5$ MeV. In our calculations, the level densities of the nuclei in their ground state were calculated by using the shell corrections E_{shell}(g.s.) of Möller *et al.* [4], while for the saddle point no shell effect was assumed, E_{shell}(saddle) = 0. (See the discussion on this question in Ref. [14].)

IV. COLD FUSION EXCITATION FUNCTIONS AND CROSS SECTIONS

The l-dependent version of the FBD model outlined above can be used to calculate excitation functions of the evaporation-residue cross section σ_{ER} given by Eq. (1). Table I shows a list of cold fusion reactions, in which different isotopes of superheavy elements of atomic numbers Z from 104 to 113 were synthesized in the bombardment of ^{208}Pb and ^{209}Bi targets with a variety of projectiles ranging from ^{48,50}Ti to ^{70}Zn [15–36]. The list contains, as independent entries, some data for the same reactions obtained in experiments carried out in different laboratories.

As an example, Fig. 1 shows the experimental excitation function for the ^{208}Pb(^{58}Fe,n)^{265}Hs reaction [15,16] compared with the results of the FBD model calculation. As discussed in Ref. [2], the rise and fall of the excitation function is due

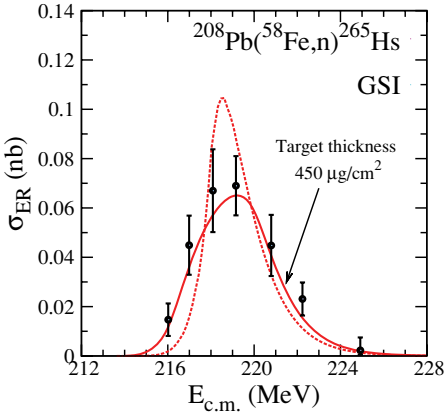

FIG. 1. (Color online) Theoretical excitation function for the ^{208}Pb(^{58}Fe,n)^{265}Hs reaction calculated with the l-dependent FBD model for infinitely thin target (dashed line) and the corresponding curve corrected for the actual target thickness (solid line), compared with experimental data [15,16]. The height of the theoretical curve, averaged over the beam energy spread due to the target thickness, is fitted to the maximum of the experimental excitation function by adjusting a value of $s_{\rm inj}$ (the injection point), the only adjustable parameter of the model.

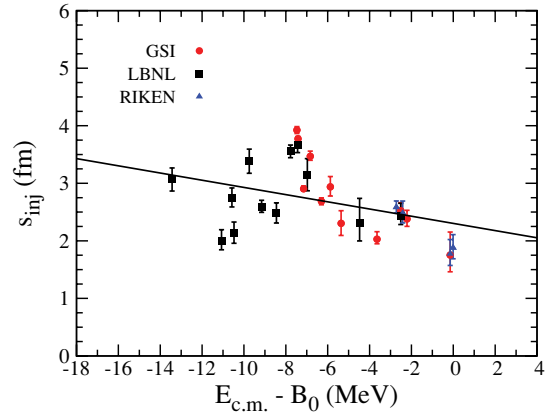

FIG. 2. (Color online) The injection point distances $s_{\rm inj}$ deduced from fitting predictions of the FBD model to 27 excitation functions of cold fusion reactions listed in Table I. The $s_{\rm inj}$ values are plotted as a function of the excess of kinetic energy above the Coulomb barrier, $E_{\rm c.m.} - B_0$. A least-square linear fit, $s_{\rm inj} \approx 2.30$ fm $- 0.062(E_{\rm c.m.} - B_0)$ fm/MeV, is shown by the solid line.

to the rising capture cross section above the energy threshold determined by the Q value of the $1n$ reaction channel,

$$E_{\rm c.m.}^{\rm thresh} = -Q(1n) = (M_{A-1} + M_n - M_P - M_T)c^2, \qquad (38)$$

combined with the rising $P_{\rm fus}$ factor, both counterbalanced by the factor $P_<$ sharply decreasing above the threshold for second chance fission [see Eq. (32)]. Therefore the maximum of the excitation function is expected to be located near the energy corresponding to the top of the fission barrier of the nucleus $(A-1)$, B_f^{A-1}:

$$E_{\rm c.m.}^{\rm max} \approx B_f^{A-1} + (M_{A-1} + M_n - M_P - M_T)c^2. \qquad (39)$$

In the above expressions M_T, M_P, M_n, and M_{A-1} stand for the target mass, projectile mass, neutron mass, and daughter-nucleus mass, respectively.

The plot in Fig. 1 is displayed in the linear scale to emphasize discrepancies between the calculated excitation function and the measured cross sections. The dashed line is calculated for an infinitely thin target. In real experiments the beam loses its energy while passing through the target, so the fusion reaction may occur within a range of energies $E \pm \frac{1}{2}\Delta E$, where E corresponds to the energy at the center of target, and ΔE is the loss of the beam kinetic energy in the target (converted to the scale of the center-of-mass energies). For typical target thicknesses used in experiments listed in Table I, ΔE was about 3–5 MeV. In order to compare the model predictions with experimental excitation function, for each point of the theoretical curve at an energy E, the calculated cross section has to be averaged over the energy range from $E - \frac{1}{2}\Delta E$ to $E + \frac{1}{2}\Delta E$. The resulting theoretical curve is decreased and wider than for the infinitely thin target, as shown by the solid curve in Fig. 1.

The height of the target-thickness-corrected curve has to be compared now with the data points of the experimental excitation function. The FBD model contains only one adjustable parameter, namely, the injection-point distance $s_{\rm inj}$, from where the fusing system starts its climb uphill in the process of thermal fluctuations to overcome the saddle point and to form the compound nucleus. (We remind readers that the variable s is the excess of length of the system at a given configuration over the sum of the projectile and target diameters; see Sec. IIC.) By fitting the hight of the theoretical curve (averaged over the target thickness) to the maximum of the experimental excitation function we determine a value of $s_{\rm inj}$ for a given reaction.

Figure 2 shows the compilation of the deduced $s_{\rm inj}$ values for the whole set of analyzed reactions. They range from about 1.8 to 3.8 fm. This means, in accordance with the definition of s mentioned above, that the deduced length of the colliding system at the injection point exceeds the length of the target plus projectile system by 1.8–3.8 fm. The deduced values of $s_{\rm inj}$ are plotted in Fig. 2 as function of the excess of kinetic energy above the Coulomb barrier, $E_{\rm c.m.} - B_0$. Such a dependence might be expected on the grounds of classical trajectory calculations. However, only a weak trend of slowly decreasing $s_{\rm inj}$ with the increasing energy is observed,

$$s_{\rm inj} \approx 2.30 \text{ fm} - 0.062(E_{\rm c.m.} - B_0) \text{ fm/MeV}. \qquad (40)$$

One can observe that the deduced $s_{\rm inj}$ values are dispersed much more than would result from the error bars based only on the statistics of the cross section measurements. Nevertheless, the trend of the decreasing $s_{\rm inj}$ values with the increasing energy seems to be really present in the data. This trend should be established more precisely in future analysis of hot fusion reactions that cover a wider energy range. We adopt the linear expression for $s_{\rm inj}$, Eq. (40), as the only adjustable input to the model.

A comparison of the experimentally measured excitation functions for 12 selected reactions with the corresponding theoretical curves is shown in Fig. 3. Solid curves show

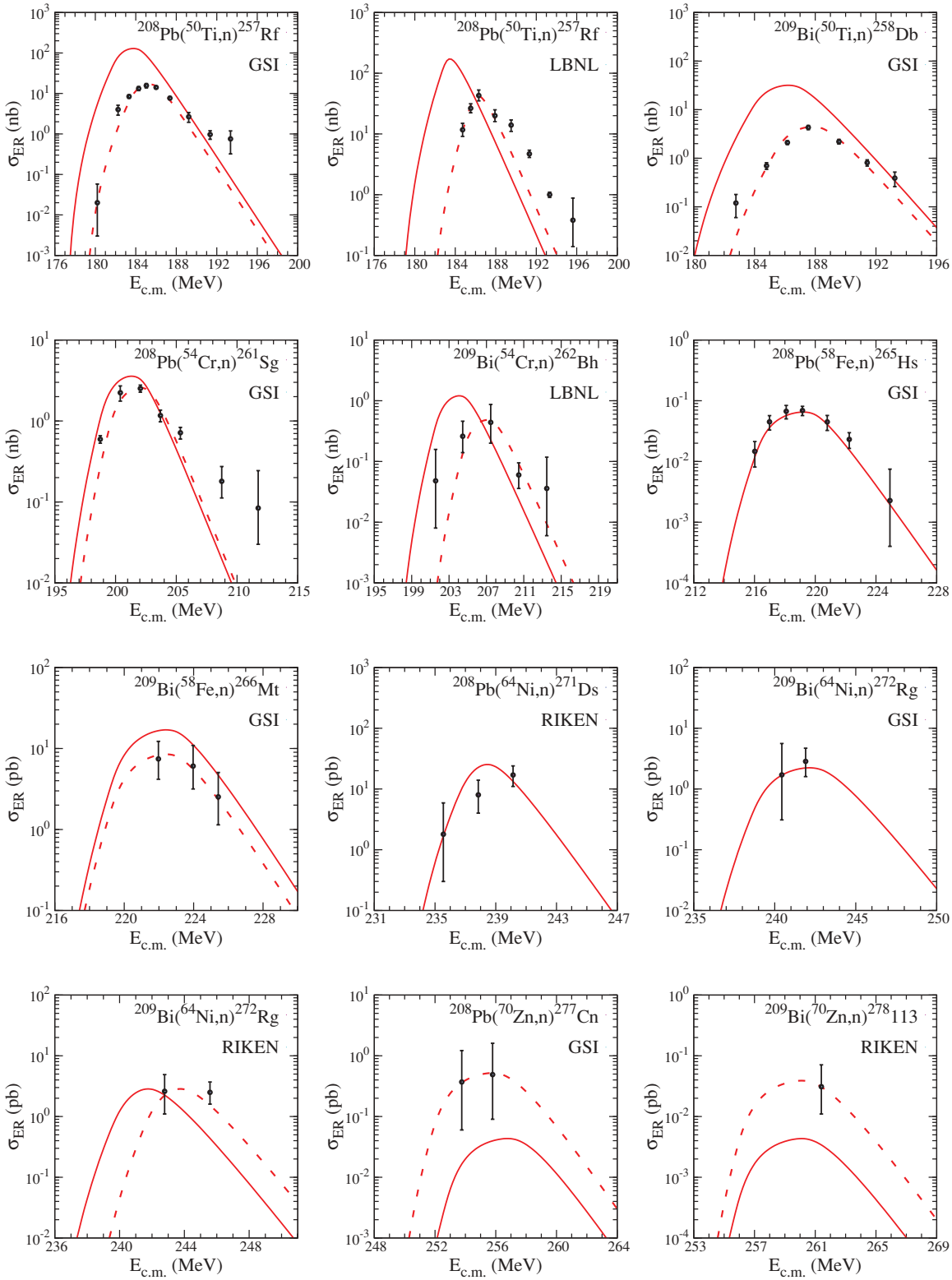

FIG. 3. (Color online) Comparison of the measured excitation functions for 12 selected cold fusion reactions (for references see Table I) with predictions of the l-dependent FBD model assuming s_{inj} values given by Eq. (40). Solid curves represent predictions accounting for the effect of the beam energy smearing due to the target thickness. Dashed lines show the theoretical curves shifted in energy and multiplied by a factor to fit the experimental points (see text).

predictions of the new version of the FBD model calculated according to Eq. (1), with the empirically found approximation for $s_{\rm inj}$ given by Eq. (40). The theoretical curves have been averaged over the energy range ΔE accounting for the target thickness, as described above. Values of the target thickness, reported in the listed papers, are given in Table I.

The first two panels in Fig. 3 present data and results of calculations for the same reaction, ^{208}Pb(^{50}Ti,n)^{257}Rf, with the excitation function taken for a thick (400 μg/cm^2) and a thin (104 μg/cm^2) target. A difference in the width of the excitation functions is clearly seen. Dashed lines in all panels of Fig. 3 show the theoretical curves (solid lines) shifted in energy and multiplied by a factor to fit the experimental points. For most of lighter elements, the necessary energy shifts turned out to be about 2–3 MeV (usually toward higher energies), while for the heaviest elements the predicted positions of the maxima do not show such a systematic shift. The multiplying factors range from 0.3 to 3. A degree of agreement of the solid and dashed curves is a measure of the accuracy of the model predictions regarding both the location of the maximum of the excitation function and the absolute value of the cross section.

Figure 4 presents the compilation of the peak positions of the excitations functions measured in all 27 experiments (carried out in GSI Darmstadt, LBNL Berkeley, and RIKEN Tokyo), which are listed in Table I. The peak energy (or the energy of a single measurement for the heaviest elements) is plotted in Fig. 4 as a function of the Coulomb interaction parameter $z = Z_1 Z_2/(A_1^{1/3} + A_2^{1/3})$, which is a convenient quantity to systemize the studied fusion reactions. The theoretical peak positions of the excitation functions calculated with the FBD model are joined by the solid line in Fig. 4.

As discussed earlier, the maximum of the excitation function is expected to be located near the energy corresponding

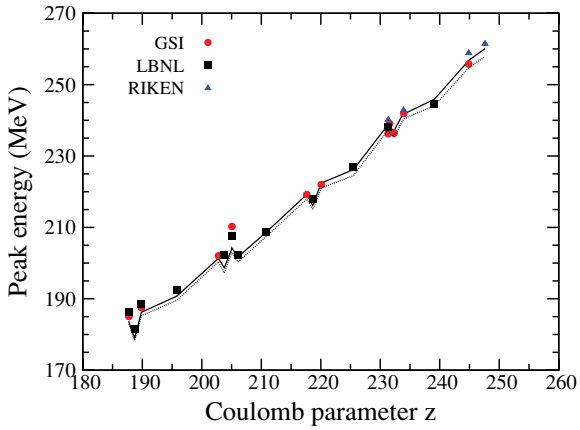

FIG. 4. (Color online) Peak positions of the experimental excitation functions (circles, squares and triangles) compared with the l-dependent FBD model predictions and plotted as a function of the Coulomb interaction parameter z. The dotted line shows an approximation to the peak position corresponding to the top of the fission barrier of the final nucleus after the neutron emission, given by Eq. (39). The exact theoretical peak position is shown by the solid line.

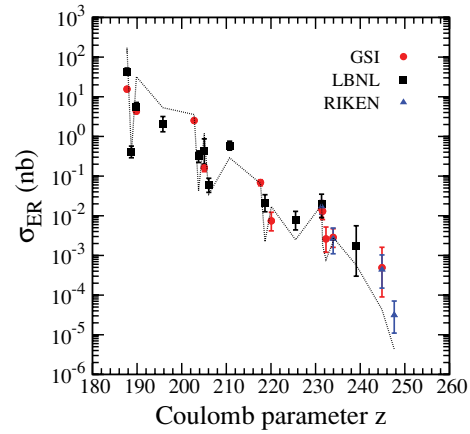

FIG. 5. (Color online) Complete set of measured cross sections (at the maximum of the excitation function) for cold fusion reactions (see Table I), plotted as a function of the Coulomb interaction parameter z, and compared with the l-dependent FBD model predictions (dotted line).

to the top of the fission barrier of the final nucleus of the mass number $A-1$, and thus given by Eq. (39). This position depends only on the ground-state masses of the projectile, target, and the final nucleus after the neutron emission and on the fission barrier B_f^{A-1}. Figure 4 presents the "optimum energies" [1,2] prescribed by Eq. (39) and shown by the dotted line. It is seen that the approximate formula of Eq. (39) approximates very well the exact theoretical peak positions represented by the solid line.

It should be noted that Eq. (39) gives at least a potential possibility to directly measure the fission barrier height B_f^{A-1} of the final nucleus $A-1$, provided its ground-state mass M_{A-1} is known. In practice it will require a considerable improvement of the precision of the beam energy determination, which in the present-time experiments is of about $\pm$2–3 MeV, but potentially it offers an important tool for verification of theoretical models, especially in light of large discrepancies between the fission barriers of superheavy nuclei predicted by Möller *et al.* [37] and Kowal *et al.* [38].

Having discussed the predictions of the optimum bombarding energy, we pass to predictions of the cross sections for the production of the final compound-residue nuclei. In Fig. 5 we present the complete set of the measured cross sections (at the maximum of the excitation function) for all the cold fusion reactions listed in Table I. The cross sections are plotted as a function of the Coulomb interaction parameter z and compared with our FBD model predictions. The theoretical values of the cross section are visualized by the dotted line. (Particular reactions can be identified in Fig. 5 according to their z values, which are listed in Table I together with respective references.) The calculated cross sections agree quite well with the experimental values in a wide range of cross sections varying over six orders of magnitude from several tens of nanobarns to tens of femtobarns. It is interesting to note that the theoretical cross sections, when plotted as a function of z, clearly show structure effects characterizing individual combinations of the target and projectile used to synthesize a given superheavy nucleus. Figure 5 demonstrates that the

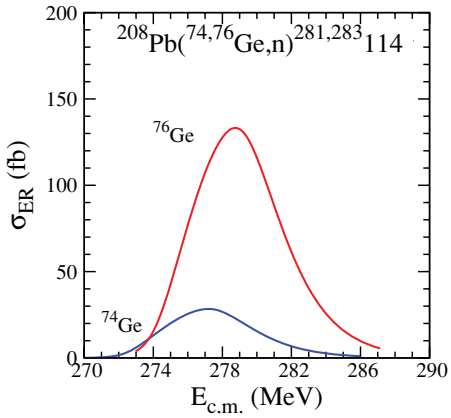

FIG. 6. (Color online) Two excitation functions for the synthesis of $Z = 114$ nuclei in cold fusion reactions ^{208}Pb(^{74,76}Ge,n)^{281,283}114, predicted with the l-dependent FBD model. The excitation functions are averaged over the assumed beam energy spread corresponding to a thick target of $\Delta E = 5$ MeV.

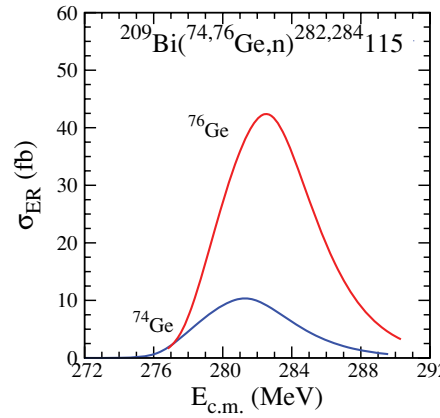

FIG. 7. (Color online) Two excitation functions for the synthesis of $Z = 115$ nuclei in cold fusion reactions ^{209}Bi(^{74,76}Ge,n)^{282,284}115, predicted with the l-dependent FBD model. The excitation functions are averaged over the assumed beam energy spread corresponding to a thick target of $\Delta E = 5$ MeV.

measured cross sections evidently are correlated with these entrance channel effects.

A review of the cross sections for the production of superheavy nuclei in cold fusion reactions, presented in Fig. 5, demonstrates that this class of fusion reactions practically cannot be extended for the synthesis of superheavy nuclei beyond, say, $Z = 115$. For the element $Z = 113$ a record low cross section of about 30 fb had been reached [35,36]. As demonstrated in the series of discovery experiments by Oganessian *et al.* (see the review article [39]), heavier superheavy elements of $Z = 114$–118 are easier to reach in hot fusion reactions, especially in those induced by ^{48}Ca projectiles bombarding heavy actinide targets.

On the other hand, the cold fusion reactions remain the only way to reach new nuclides in the empty, unexplored region of the chart of nuclides located in the *neutron-deficient* side of the decay products of elements 114–118 discovered in hot fusion reactions [39]. Specifically, we have in mind reactions on ^{208}Pb and ^{209}Bi targets induced by ^{74,76}Ge projectiles leading to the synthesis of ^{281,283}114 and ^{282,284}115 nuclides in cold fusion ($1n$) reactions. The predicted excitation functions for these reactions are shown in Figs. 6 and 7. The ^{208}Pb(^{76}Ge,n)^{283}114 reaction seems to be especially promising, showing the peak cross section of about 130 fb at $E_{\mathrm{c.m.}} \approx 278$ MeV, i.e., achievable in very sensitive subpicobarn experiments such as those of Refs. [35,36]. Thus, if the ^{283}114 nuclide were successfully formed, the chain of its α decays would significantly fill the present gap between the area of the heaviest nuclei, products of the decay of elements 114–118, and better-known decay products of cold fusion ($1n$) reactions explored so far.

In conclusion, the present version of the FBD model satisfactorily describes all the experimental data on cold fusion reactions in which superheavy nuclei of $Z \leqslant 113$ were produced in (fusion,$1n$) reactions. This well tested l-dependent version of the FBD model can be used for planning future experiments in attempts to produce new nuclides accessible in the cold fusion reactions. The model is suitable to easily choose an optimum combination of the target and projectile to synthesize a given nuclide, to predict the optimum bombarding energy and the production cross section. Moreover, having in mind the prospect of future experiments with precisely known beam energies, the FBD model can be helpful for experimental determination of the fission barrier heights from peak positions of the excitation functions.

Having tested particular components of the FBD model in the domain of relatively simple cold fusion ($1n$) reactions, one can attempt to generalize this model for the class of hot fusion (xn) reactions, the only way to reach the unsynthesized yet heaviest elements of $Z = 119$, 120, and beyond.

ACKNOWLEDGMENTS

We would like to especially thank the late Władysław Świątecki for many insightful discussions and encouragement. KSW and JW thank the Heavy Elements group led by Heino Nitsche for the hospitality extended to us during our visit to the Lawrence Berkeley National Laboratory. We especially thank Kenneth Gregorich and Jackie Gates for numerous discussions. We also thank Adam Sobiczewski, Zygmunt Patyk, and Michał Kowal for providing us with details of their macroscopic-microscopic model calculations of fission barriers and saddle-point deformations.

[1] W. J. Świątecki, K. Siwek-Wilczyńska, and J. Wilczyński, Acta Phys. Pol. B **34**, 2049 (2003).

[2] W. J. Świątecki, K. Siwek-Wilczyńska, and J. Wilczyński, Phys. Rev. C **71**, 014602 (2005).

[3] K. Siwek-Wilczyńska and J. Wilczyński, Phys. Rev. C **69**, 024611 (2004).
[4] P. Möller, J. R. Nix, W. D. Myers, and W. J. Swiatecki, At. Data Nucl. Data Tables **59**, 185 (1995).
[5] H. Riske, *The Fokker-Planck Equation* (Springer-Verlag, Berlin, 1989).
[6] J. Blocki and W. J. Swiatecki, Lawrence Berkeley Laboratory preprint LBL-12811, May 1982 (unpublished).
[7] W. D. Myers and W. J. Swiatecki, Ark. Fys. **36**, 343 (1967).
[8] W. D. Myers and W. J. Swiatecki, Lawrence Berkeley Laboratory preprint LBL-36803, December 1994 (unpublished), available at [http://ie.lbl.gov/txt/ms.txt].
[9] R. W. Hasse and W. D. Myers, *Geometrical Relationships of Macroscopic Nuclear Physics* (Springer-Verlag, Berlin, 1988).
[10] I. Muntian, Z. Patyk, and A. Sobiczewski, Yad. Fiz. **66**, 1051 (2003); Phys. At. Nucl. **66**, 1015 (2003); Acta Phys. Pol. B **34**, 2141 (2003).
[11] R. Vandenbosch and J. R. Huizenga, *Nuclear Fission* (Academic Press, New York, 1973), p. 229.
[12] W. Reisdorf, Z. Phys. A **300**, 227 (1981).
[13] A. V. Ignatyuk, G. N. Smirenkin, and A. S. Tishin, Yad. Fiz. **21**, 485 (1975); Sov. J. Nucl. Phys. **21**, 255 (1975).
[14] K. Siwek-Wilczyńska, I. Skwira, and J. Wilczyński, Phys. Rev. C **72**, 034605 (2005).
[15] S. Hofmann *et al.*, Nucl. Phys. A **734**, 93 (2004).
[16] S. Hofmann, Rep. Prog. Phys. **61**, 639 (1998), and private communication.
[17] I. Dragojević, K. E. Gregorich, C. E. Düllman, M. A. Garcia, J. M. Gates, S. L. Nelson, L. Stavsetra, R. Sudowe, and H. Nitsche, Phys. Rev. C **78**, 024605 (2008).
[18] F. P. Heßberger *et al.*, Eur. Phys. J. A **12**, 57 (2001).
[19] J. M. Gates *et al.*, Phys. Rev. C **78**, 034604 (2008).
[20] C. M. Folden III *et al.*, Phys. Rev. C **79**, 027602 (2009).
[21] S. L. Nelson, C. M. Folden III, K. E. Gregorich, I. Dragojević, C. E. Düllmann, R. Eichler, M. A. Garcia, J. M. Gates, R. Sudowe, and H. Nitsche, Phys. Rev. C **78**, 024606 (2008).
[22] G. Münzenberg *et al.*, Z. Phys. A **333**, 163 (1989).
[23] S. L. Nelson, K. E. Gregorich, I. Dragojević, M. A. Garcia, J. M. Gates, R. Sudowe, and H. Nitsche, Phys. Rev. Lett. **100**, 022501 (2008).
[24] C. M. Folden III, S. L. Nelson, C. E. Düllmann, J. M. Schwantes, R. Sudowe, P. M. Zielinski, K. E. Gregorich, H. Nitsche, and D. C. Hoffman, Phys. Rev. C **73**, 014611 (2006).
[25] I. Dragojević, K. E. Gregorich, C. E. Düllmann, J. Dvorak, P. A. Ellison, J. M. Gates, S. L. Nelson, L. Stavsetra, and H. Nitsche, Phys. Rev. C **79**, 011602(R) (2009).
[26] S. Hofmann, F. P. Heßberger, V. Ninov, P. Armbruster, G. Münzenberg, C. Stodel, A. G. Popeko, A. V. Yeremin, S. Saro, and M. Leino, Z. Phys. A **358**, 377 (1997).
[27] S. L. Nelson, K. E. Gregorich, I. Dragojević, J. Dvorak, P. A. Ellison, M. A. Garcia, J. M. Gates, L. Stavsetra, M. N. Ali, and H. Nitsche, Phys. Rev. C **79**, 027605 (2009).
[28] T. N. Ginter *et al.*, Phys. Rev. C **67**, 064609 (2003).
[29] C. M. Folden III, K. E. Gregorich, C. E. Düllmann, H. Mahmud, G. K. Pang, J. M. Schwantes, R. Sudowe, P. M. Zielinski, H. Nitsche, and D. C. Hoffman, Phys. Rev. Lett. **93**, 212702 (2004).
[30] K. Morita *et al.*, Eur. Phys. J. A **21**, 257 (2004).
[31] K. Morita *et al.*, Nucl. Phys. A **734**, 101 (2004).
[32] S. Hofmann *et al.*, Eur. Phys. J. A **10**, 5 (2001).
[33] K. Morita *et al.*, J. Phys. Soc. Jpn. **73**, 1738 (2004).
[34] K. Morita *et al.*, J. Phys. Soc. Jpn. **76**, 043201 (2007).
[35] K. Morita *et al.*, J. Phys. Soc. Jpn. **76**, 045001 (2007).
[36] K. Morita *et al.*, J. Phys. Soc. Jpn. **73**, 2593 (2004).
[37] P. Möller, A. J. Sierk, T. Ichikawa, A. Iwamoto, R. Bengtsson, H. Uhrenholt, and S. Åberg, Phys. Rev. C **79**, 064304 (2009).
[38] M. Kowal, P. Jachimowicz, and A. Sobiczewski, Phys. Rev. C **82**, 014303 (2010).
[39] Yu. Oganessian, J. Phys. G: Nucl. Part. Phys. **34**, R165 (2007).